

# First-principles investigation of high- $\kappa$ dielectrics: Comparison between the silicates and oxides of hafnium and zirconium

G.-M. Rignanese and X. Gonze

*Unité de Physico-Chimie et de Physique des Matériaux, Université Catholique de Louvain, 1 Place Croix du Sud,  
B-1348 Louvain-la-Neuve, Belgium*

*and Research Center on Microscopic and Nanoscopic Materials and Electronic Devices (CERMIN), Université Catholique de Louvain,  
B-1348 Louvain-la-Neuve, Belgium*

Gyuchang Jun

*Materials Science and Engineering Department, Stanford University, Stanford, California 94305-4040, USA*

Kyeongjae Cho

*Department of Mechanical Engineering, Stanford University, Stanford, California 94305-4040, USA*

Alfredo Pasquarello

*Institut de Théorie des Phénomènes Physiques (ITP), Ecole Polytechnique Fédérale de Lausanne (EPFL),  
CH-1015 Lausanne, Switzerland*

*and Institut Romand de Recherche Numérique en Physique des Matériaux (IRRMA), CH-1015 Lausanne, Switzerland*

(Received 8 October 2003; revised manuscript received 12 December 2003; published 25 May 2004)

Using density-functional theory, we investigate the structural, vibrational, and dielectric properties of Hf and Zr oxides and silicates which have drawn considerable attention as alternative high- $\kappa$  materials. For the silicates, we consider hafnion HfSiO<sub>4</sub> and zircon ZrSiO<sub>4</sub>; while for the oxides, we study the cubic and tetragonal phases of HfO<sub>2</sub> and ZrO<sub>2</sub>. Special emphasis is put on the analysis of the differences and similarities between Hf and Zr in these materials. In particular, we discuss the Born effective charge tensors, the phonon frequencies at the  $\Gamma$  point of the Brillouin zone, and the dielectric permittivity tensors. Our study reveals very similar properties of Hf and Zr compounds, which are essentially related to the chemical homology of Hf and Zr.

DOI: 10.1103/PhysRevB.69.184301

PACS number(s): 63.20.-e, 71.20.-b, 77.22.-d

## I. INTRODUCTION

The narrowest feature on present-day integrated circuits is the gate oxide, the thin dielectric layer that forms the basis of field-effect device structures. So far, silicon dioxide has been the dielectric of choice. The Semiconductor Industry Association's (SIA's) International Technology Roadmap for Semiconductors indicates that the equivalent thickness of the gate dielectric will need to be 1.0 nm to 1.5 nm by 2004. Due to increased power consumption, intrinsic device reliability, and circuit instabilities associated with silicon dioxide of such a small thickness (about five silicon atoms across), an alternative high-permittivity (high- $\epsilon$ ) gate dielectric with low leakage current and at least equivalent capacitance, performance, and reliability is required. Considerable research efforts have been dedicated to the study of potential dielectric-gate materials.

Various metal oxides and their silicates have been considered.<sup>1</sup> A substantial amount of investigation has gone into the group Hf and Zr silicates and oxides,<sup>1,2</sup> since these materials in the form of amorphous films are thermodynamically stable in direct contact with Si up to high temperature. Their dielectric properties constitute an issue of great practical relevance. In particular, it is highly desirable to develop a better understanding of how the permittivity is related to the underlying microstructure.

This has stimulated a series of first-principles studies.<sup>3-8</sup>

First, the crystalline Zr silicate, namely zircon, was investigated.<sup>3</sup> Next, the tetragonal phase of ZrO<sub>2</sub> was considered<sup>4</sup> and compared to the cubic phase, which had been studied previously for other reasons.<sup>9,10</sup> The study of the monoclinic phase of ZrO<sub>2</sub> (Ref. 5) completed nicely the analysis of crystalline Zr oxides. The corresponding work for crystalline Hf oxides was also the object of a thorough study.<sup>6</sup> Then, the behavior of each oxide at the interface with Si was investigated<sup>7</sup> through a hypothetical tetragonal Si-epitaxial crystalline phase obtained by imposing the in-plane lattice constant of Si and adjusting the axial ratio and internal coordinates. Finally, amorphous Zr silicates were analyzed in detail<sup>8</sup> and a microscopic scheme that relates the dielectric constants to the local bonding of Si and Zr atoms was proposed.

In principle, Hf and Zr oxides and silicates are expected to have similar physical and chemical properties due to the chemical homology of Hf and Zr: their atomic radii, ionic radii, and electronegativity values are almost identical.<sup>11</sup> For instance, in the case of ZrSiO<sub>4</sub> and HfSiO<sub>4</sub>, the similarities are such that there is complete miscibility between the two crystalline systems.<sup>12</sup> From this standpoint, the dielectric constants of tetragonal HfO<sub>2</sub>, recently calculated in Ref. 6, are somewhat surprising. Indeed, the static dielectric constant of HfO<sub>2</sub> in a direction perpendicular to the tetragonal axis was found<sup>6</sup> to be more than twice as large as that of ZrO<sub>2</sub>.<sup>4,5</sup> Furthermore, this particular dielectric constant of

tetragonal  $\text{HfO}_2$  is also much larger than those of the cubic and monoclinic phases of  $\text{HfO}_2$ .<sup>6</sup>

A deeper analysis of this surprising result might provide very useful information on how to increase the dielectric constant, which is a key issue in the framework of the quest for an alternative high-permittivity gate dielectric. This requires investigating the various contributions to the static dielectric constants which depend on the frequencies of the IR modes and their oscillator strength tensors (which are in turn related to the Born effective charge tensors and the atomic eigendisplacements).

Therefore, we set out for a comprehensive comparison between the dielectric properties of Hf and Zr silicates and oxides within density-functional theory (DFT). Since results for zircon and Zr oxides have already been obtained previously,<sup>3,4</sup> we here extend our calculations to Hf-related compounds: hafnon, cubic  $\text{HfO}_2$ , and tetragonal  $\text{HfO}_2$ . Although the results for  $\text{HfO}_2$  are already available in the literature,<sup>6</sup> we here reobtained their dielectric constants within our theoretical framework to ensure that the comparison is carried out between results obtained with the same technical ingredients. Overall, our results indicate a strong similarity between compounds based on hafnium and zirconium. The value of the static dielectric constant of tetragonal  $\text{HfO}_2$  in a direction perpendicular to tetragonal axis is found to be roughly two thirds of that of tetragonal zirconia, i.e., our results *do not confirm* the unusually large value calculated in Ref. 6. The discrepancies between the two calculations are traced back to the relevant infrared frequency and Born effective charges.

The present paper is organized as follows. After a brief description of the technical details in Sec. II, we compare the results of our calculations for various properties of Hf and Zr crystalline silicates in Sec. III. Section III A is dedicated to the study of the structural properties of hafnon and zircon. In Sec. III B, we investigate the electronic properties of these materials and present the electronic density of states. In Sec. III C, the Born effective charge tensors are analyzed in detail. The phonon frequencies at the  $\Gamma$  point of the Brillouin zone are discussed in Sec. III D, while the dielectric permittivity tensors for the two silicates are compared in Sec. III E. Section IV is devoted to the cubic and tetragonal phases of  $\text{ZrO}_2$  and  $\text{HfO}_2$ . Our results are presented in parallel with those of Refs. 5 and 6. We discuss the structural parameters of these compounds in Sec. IV A, the Born effective charge tensors in Sec. IV B, and the phonon frequencies at the  $\Gamma$  point of the Brillouin zone in Sec. IV C. The respective dielectric permittivity tensors are analyzed in detail in Sec. IV D. Finally, in Sec. V, we summarize our results and conclude.

## II. TECHNICAL DETAILS

All our calculations are performed using the ABINIT package, developed by the authors and collaborators.<sup>13</sup> The exchange-correlation energy is evaluated within the local-density approximation (LDA) to DFT, using Perdew-Wang's parametrization<sup>14</sup> of Ceperley-Alder electron-gas data.<sup>15</sup>

Only valence electrons are explicitly considered using

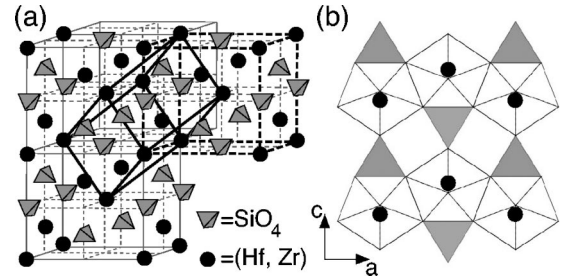


FIG. 1. Structure of hafnon and zircon. (a) The individual  $\text{SiO}_4$  units are represented schematically by the gray tetrahedra, while  $M=(\text{Hf}, \text{Zr})$  atoms are indicated by black spheres. The two sets of dashed lines and heavy lines outline the body-centered-tetragonal unit cell and the primitive cell, respectively. (b) Besides the  $\text{SiO}_4$  units, the  $\text{MO}_8$  triangular dodecahedra with the  $M$  atoms in their center are also drawn.

pseudopotentials to account for core-valence interactions. We use norm-conserving pseudopotentials<sup>16,17</sup> with  $\text{Hf}(5s, 5p, 5d, 6s)$ ,  $\text{Zr}(4s, 4p, 4d, 5s)$ ,  $\text{Si}(3s, 3p)$ , and  $\text{O}(2s, 2p)$  levels treated as valence states. The pseudopotentials are generated using the following atomic valence configurations:  $\text{Hf}(5s^2 5p^6 5d^2 6s^2)$ ,  $\text{Zr}(4s^2 4p^6 4d^2 5s^0)$ ,  $\text{Si}(3s^2 3p^2)$ , and  $\text{O}(2s^2 2p^4)$ . In the case of Hf, we take core radii of 1.50, 2.85, 2.45, 3.50 a.u. for describing angular waves from  $s$  to  $f$ . The corresponding values for the Zr pseudopotential (up to the  $d$  wave) are 1.75, 1.55, and 1.70 a.u. For the Si pseudopotential, the same cutoff radius of 2.00 a.u. is used for the three lowest angular-momentum waves. For the O pseudopotential, we use a cutoff radius of 1.50 a.u. for both  $s$  and  $p$  waves. We adopted a separable form for the pseudopotentials<sup>18</sup> treating the following angular-momentum waves as local:  $f$  for Hf,  $d$  for Zr,  $d$  for Si, and  $p$  for O.

The wave functions are expanded in plane waves up to a kinetic-energy cutoff of 30 Ha. The chosen kinetic-energy cutoff and  $k$ -point sampling of the Brillouin-zone ensure convergence of all the calculated properties.

## III. CRYSTALLINE SILICATES

### A. Structural properties

Hafnon and zircon have a conventional unit cell which is body-centered tetragonal (space group  $I4_1/amd$ , No. 141) and contains four formula units of  $M\text{SiO}_4$  with  $M=(\text{Hf}, \text{Zr})$ , as illustrated by the dashed lines in Fig. 1(a). A primitive cell containing only two formula units of  $M\text{SiO}_4$  can also be defined, as indicated by the heavy lines in Fig. 1(a).

The structure of hafnon and zircon may be viewed as consisting of  $(\text{SiO}_4)^{4-}$  anions and  $M^{4+}$  cations with  $M=(\text{Hf}, \text{Zr})$ , as illustrated by the gray tetrahedra and the black spheres in Fig. 1(a). This is consistent with the larger bond length (about 25%) of the  $M$ -O compared to the Si-O bond. The experimental data describing the structure of hafnon<sup>12</sup> and zircon<sup>19</sup> are reported in Table I.

Alternatively, as presented in Fig. 1(b), a different view may be adopted in which  $\text{HfSiO}_4$  and  $\text{ZrSiO}_4$  consist of alternating (discrete)  $\text{SiO}_4$  tetrahedra and  $\text{MO}_8$  units, sharing edges to form chains parallel to the  $c$  direction. Note that in

TABLE I. Structural parameters of  $\text{HfSiO}_4$  and  $\text{ZrSiO}_4$ . The length unit is the Angstrom. The theoretical results for  $\text{ZrSiO}_4$  are those of Ref. 3. The experimental data are taken from Ref. 12 for  $\text{HfSiO}_4$ , and from Ref. 19 for  $\text{ZrSiO}_4$ .

	$\text{HfSiO}_4$		$\text{ZrSiO}_4$	
	Theor.	Expt.	Theor.	Expt.
$a$	6.61	6.57	6.54	6.61
$c$	5.97	5.96	5.92	6.00
$u$	0.0672	0.0655	0.0645	0.0646
$v$	0.1964	0.1948	0.1945	0.1967
Volume	130.42	128.63	126.60	131.08
$d(\text{Si-O})$	1.62	1.61	1.61	1.62
$d(\text{M-O})$	2.14	2.10	2.10	2.13
	2.27	2.24	2.24	2.27
$\angle(\text{O-Si-O})$	97°	97°	97°	97°
	116°	117°	116°	116°

these  $\text{MO}_8$  units four O atoms are closer to the  $M$  atom than the four other ones (about 6% difference in the  $M$ -O bond length, see Table I).

The positions of the  $M=(\text{Hf}, \text{Zr})$  and Si atoms are imposed by symmetry: they are located at  $(0, \frac{3}{4}, \frac{1}{8})$  and  $(0, \frac{1}{4}, \frac{3}{8})$  on the  $4a$  and  $4b$  Wyckoff sites, respectively. The O atoms occupy the  $16h$  Wyckoff sites  $(0, u, v)$ , where  $u$  and  $v$  are internal parameters.

Table I summarizes our results obtained after relaxation of the lattice constants and the internal cell parameters. The calculated lattice constants  $a$  and  $c$ , as well as the internal parameters  $u$  and  $v$  are found to be in excellent agreement with their corresponding experimental values.<sup>12,19</sup> Interatomic distances and angles are within one or two percent of the experimental values. This accuracy is largely sufficient to address in a meaningful way the dynamical and dielectric properties.

### B. Electronic structure

In Fig. 2, we present the calculated electronic density of states (DOS) for hafnon and zircon. The complete electronic band structure for  $\text{ZrSiO}_4$  along several directions in the Brillouin zone can be found elsewhere.<sup>3</sup> For  $\text{HfSiO}_4$ , the

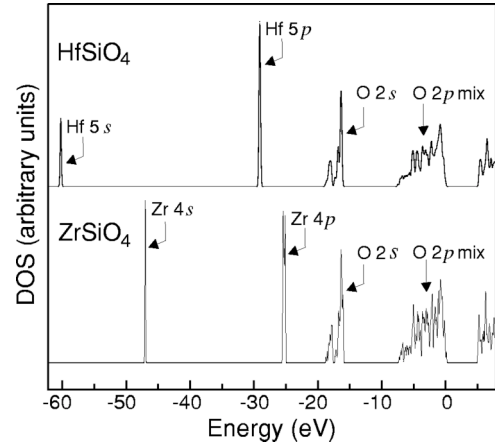


FIG. 2. Electronic density of states (DOS) for  $\text{HfSiO}_4$  and  $\text{ZrSiO}_4$ .

electronic band structure is very similar apart from the position of the Hf  $5s$  and  $5p$  bands, as explained below.

We clearly distinguish four groups in the DOS of the valence bands, of which the three lowest ones are rather peaked (small dispersion of the bands), indicative of a weak hybridization. The DOS of hafnon (zircon) exhibits a very sharp peak at  $-60.2$  eV ( $-47.1$  eV) attributed to the Hf  $5s$  (Zr  $4s$ ) states, corresponding to two flat bands in the band structure.<sup>3</sup> The peak at  $-29.8$  eV for hafnon ( $-25.5$  eV for zircon) is related to the Hf  $5p$  (Zr  $4p$ ) states: it includes six electrons per unit cell. The O  $2s$  peak (8 electrons per unit cell) is located between  $-18.0$  and  $-16$  eV for both hafnon and zircon.

By contrast, the fourth group (24 electrons per unit cell) has a much wider spread of 8 eV. These states have mainly an O  $2p$  character with some mixing of Si and  $M=(\text{Hf}, \text{Zr})$  orbitals. This mixed covalent-ionic bonding of  $\text{HfSiO}_4$  and  $\text{ZrSiO}_4$ , appearing in this group of valence bands, should be kept in mind when interpreting the Born effective charge tensors.

### C. Born effective charge tensors

The Born effective charge tensors of  $M=(\text{Hf}, \text{Zr})$ , Si, and O atoms are reported in Table II. The local site symmetry of

TABLE II. Nonvanishing components of the calculated Born effective charge tensors for  $M=(\text{Hf}, \text{Zr})$ , Si, and O atoms in  $\text{HfSiO}_4$  and  $\text{ZrSiO}_4$ . For the  $M=(\text{Hf}, \text{Zr})$  and Si atoms, the tensors are diagonal and only the principal elements are given. For the O atom located at  $(0, u, v)$ , the full tensor is reported and the principal values of its symmetric part are indicated between brackets.

Atom	$\text{HfSiO}_4$	$\text{ZrSiO}_4^a$
$M$	(+5.28+5.28+4.68)	(+5.41+5.41+4.63)
Si	(+3.18+3.18+4.35)	(+3.25+3.25+4.42)
O	$\begin{pmatrix} -1.15 & 0 & 0 \\ 0 & -3.08 & -0.19 \\ 0 & -0.35 & -2.26 \end{pmatrix}$	$\begin{pmatrix} -1.15 & 0 & 0 \\ 0 & -3.17 & -0.16 \\ 0 & -0.34 & -2.25 \end{pmatrix}$
	[-1.15 -3.16 -2.18]	[-1.15 -3.23 -2.19]

<sup>a</sup>From Ref. 3.

$M=(\text{Hf}, \text{Zr})$  and Si atoms is rather high ( $\bar{4}m2$ ). The Born effective charge tensors of  $M=(\text{Hf}, \text{Zr})$  and Si atoms are diagonal and have only two independent components: parallel and perpendicular to the tetragonal axis,  $Z_{\parallel}^*$  and  $Z_{\perp}^*$ , respectively. In contrast, the local site symmetry of the O atoms has only a mirror plane. As a consequence, the Born effective charge tensors of O atoms are not diagonal, and depend on five independent quantities. The tensor reported in Table II is for the O atom located at  $(0, u, v)$ . For the other oxygen atoms, the Born effective charge tensors can be obtained using the symmetry operations. Qualitatively, the Born effective charge tensors are very similar for  $\text{HfSiO}_4$  and  $\text{ZrSiO}_4$ . Therefore, the analysis proposed in Ref. 3 for zircon also holds for hafnion. On the one hand, important deviations are observed from the nominal ionic charges [ $+4$  for  $M=(\text{Hf}, \text{Zr})$  and Si,  $-2$  for O] indicating a mixed covalent-ionic bonding,<sup>20</sup> as already suggested by the  $M$ -O  $2p$  hybridization discussed in Sec. III B. On the other hand, the Born effective charge tensors for O atoms are very anisotropic with one component of magnitude much smaller than 2 and much smaller than the two other ones, as already observed for  $\text{SiO}_2$ -stishovite<sup>21</sup> and  $\text{TiO}_2$ -rutile.<sup>22</sup>

More quantitatively, we note that  $Z_{\perp}^*$  is about 3% smaller for hafnion in  $\text{HfSiO}_4$  than for zirconium in  $\text{ZrSiO}_4$ . The Born effective charge of Si atoms for directions perpendicular to the tetragonal axis shows a very similar behavior: it is about 2% smaller in hafnion than in zircon. For the Born effective charge in the direction parallel to the  $c$  axis, we find for Si atoms the same trend as for perpendicular directions, but the opposite one for  $M=(\text{Hf}, \text{Zr})$  atoms, the Born effective charges for Hf in hafnion being about 1% higher than for Zr in zircon. On the contrary, the Born effective charges of O atoms are very similar in  $\text{HfSiO}_4$  and  $\text{ZrSiO}_4$ . A significant difference is only observed for the second principal value, which is 2% smaller in hafnion than in zircon.

#### D. Phonon frequencies at the $\Gamma$ point

We here address the phonon frequencies at the  $\Gamma$  point of the Brillouin zone for hafnion and zircon. The theoretical group analysis predicts the following irreducible representations of optical and acoustical zone-center modes:

$$\Gamma = \underbrace{2A_{1g} \oplus 4B_{1g} \oplus B_{2g} \oplus 5E_g}_{\text{Raman}} \oplus \underbrace{3A_{2u} \oplus 4E_u}_{\text{IR}} \\ \oplus \underbrace{A_{2u} \oplus E_u}_{\text{Acoustic}} \oplus \underbrace{B_{1u} \oplus A_{2g} \oplus A_{1u} \oplus 2B_{2u}}_{\text{Silent}}.$$

Because of the nonvanishing components of the Born effective charge tensors, the dipole-dipole interaction must be properly included in the calculation of the interatomic force constants.<sup>23–25</sup> In particular, the dipole-dipole contribution is found to be responsible for the splitting between the longitudinal optic (LO) and transverse optic (TO) modes  $E_u$  and  $A_{2u}$  at the  $\Gamma$  point.

In Table III, the calculated phonon frequencies are compared with experimental values. For hafnion, experimental data are only available for Raman modes, in the form of two

TABLE III. Fundamental frequencies of  $\text{HfSiO}_4$  and  $\text{ZrSiO}_4$  (in  $\text{cm}^{-1}$ ) with their symmetry assignments. The theoretical results for  $\text{ZrSiO}_4$  are those of Ref. 3. The experimental values are taken from Ref. 27 for  $\text{HfSiO}_4$  (Raman modes only), and from Ref. 28 for  $\text{ZrSiO}_4$ .

Mode	$\text{HfSiO}_4$		$\text{ZrSiO}_4$	
	Theor.	Expt.	Theor.	Expt.
<b>Raman</b>				
$A_{1g}(1)$	462	450	442	439
$A_{1g}(2)$	970	984	971	974
$B_{1g}(1)$	162	157	225	214
$B_{1g}(2)$	395	401	397	393
$B_{1g}(3)$	638	620	632	
$B_{1g}(4)$	1016	1020	1017	1008
$B_{2g}$	247	267	252	266
$E_g(1)$	161	148	194	201
$E_g(2)$	204	212	225	225
$E_g(3)$	369	351	375	357
$E_g(4)$	530		536	547
$E_g(5)$	923		923	
<b>Infrared</b>				
$A_{2u}(\text{TO1})$			348	338
$A_{2u}(\text{LO1})$			476	480
$A_{2u}(\text{TO2})$			601	608
$A_{2u}(\text{LO2})$			646	647
$A_{2u}(\text{TO3})$			980	989
$A_{2u}(\text{LO3})$			1096	1108
$E_u(\text{TO1})$			285	287
$E_u(\text{LO1})$			341	352
$E_u(\text{TO2})$			383	389
$E_u(\text{LO2})$			420	419
$E_u(\text{TO3})$			422	430
$E_u(\text{LO3})$			466	471
$E_u(\text{TO4})$			867	885
$E_u(\text{LO4})$			1029	1035
<b>Silent</b>				
$B_{1u}$			120	
$A_{2g}$			242	
$A_{1u}$			392	
$B_{2u}(1)$			566	
$B_{2u}(2)$			943	

sets of measurements.<sup>26,27</sup> Since the agreement with both sets of data is excellent, we here only report the most recent data.<sup>27</sup> For zircon, both Raman and IR active modes have been studied experimentally,<sup>28</sup> the IR data being confirmed by more recent experiments.<sup>29,30</sup>

Overall, the agreement between theory and experiment is excellent, with a rms absolute deviation of  $4.1 \text{ cm}^{-1}$  for  $\text{HfSiO}_4$  ( $9.4 \text{ cm}^{-1}$  for  $\text{ZrSiO}_4$ ), and a rms relative deviation of 4.2% (2.5%). We obtain four Raman active modes that could not be detected experimentally: two for hafnion (at  $530 \text{ cm}^{-1}$  [ $E_g(4)$ ] and  $923 \text{ cm}^{-1}$  [ $E_g(5)$ ]) and two for zircon (at  $632 \text{ cm}^{-1}$  [ $B_{1g}(3)$ ] and  $923 \text{ cm}^{-1}$  [ $E_g(5)$ ]).

It is quite interesting to compare the phonon frequencies calculated for  $\text{HfSiO}_4$  and  $\text{ZrSiO}_4$  (see Table III). There are

TABLE IV. Electronic and static dielectric tensors of HfSiO<sub>4</sub> and ZrSiO<sub>4</sub>. The contributions of individual phonon modes to the static dielectric tensor are indicated. The tensors are diagonal and have different components parallel ( $\parallel$ ) and perpendicular ( $\perp$ ) to the  $c$  axis. The phonon mode contributions to  $\epsilon_0^\parallel$  come from the three IR-active  $A_{2u}$  modes, while the contributions to  $\epsilon_0^\perp$  come from the four IR-active  $E_u$  modes.

	HfSiO <sub>4</sub>		ZrSiO <sub>4</sub> <sup>a</sup>	
	$\parallel$	$\perp$	$\parallel$	$\perp$
$\epsilon_\infty$	4.11	3.88	4.26	4.06
$\Delta\epsilon_1$	4.93	4.38	5.90	5.16
$\Delta\epsilon_2$	0.81	0.75	0.52	1.31
$\Delta\epsilon_3$	0.80	0.35	0.85	0.05
$\Delta\epsilon_4$		1.27		1.38
$\epsilon_0$	10.65	10.63	11.53	11.96

<sup>a</sup>From Ref. 3.

several possible origins for the variations that are observed: structural changes (e.g., the volume), variation of the mass of the metal ion (ratio Hf/Zr=1.96), and differences in interatomic force constants. Given the small structural changes reported in Table I, we suspect that their effect should be very small. In order to check this, we compute the phonon frequencies for hafnion assuming that the interatomic force constants are the same as those for zircon, while the volume is allowed to vary. This analysis shows that the structural changes play a very minor role, in agreement with our intuition. The effect of the mass ratio is clear for the  $B_{1g}(1)$  mode in which the  $M=(\text{Hf}, \text{Zr})$  atoms move significantly more than O atoms: the frequency increases by about 28% in ZrSiO<sub>4</sub>. On the contrary, the frequencies should not vary much from HfSiO<sub>4</sub> to ZrSiO<sub>4</sub> for modes in which the  $M=(\text{Hf}, \text{Zr})$  atoms are not involved [i.e., all the silent modes,  $A_{1g}(1)$  and (2), and  $B_{2g}$ ], as well as for those in which the O atoms move significantly more than the  $M=(\text{Hf}, \text{Zr})$  atoms. In most of these cases, this is indeed what is observed. However, there are a few significant exceptions: for instance, the  $B_{1u}$  mode for which the frequency increases by about 11%. These are cases in which the effects due to differences in the interatomic force constants are dominant.

### E. Dielectric permittivity tensors

Due to the tetragonal symmetry of the hafnion and zircon crystals, the electronic ( $\epsilon_\infty$ ) and static ( $\epsilon_0$ ) permittivity tensors have two independent components  $\epsilon_\parallel$  and  $\epsilon_\perp$ , parallel and perpendicular to the  $c$  axis, respectively. The calculated values of  $\epsilon_\infty$  and  $\epsilon_0$  are reported in Table IV.

For zircon, the theoretical values are larger than the experimental ones by about 10%,<sup>3</sup> as often found in the LDA to density-functional theory. For hafnion, we were not able to find accurate measurements in the literature. For hafnium silicates, values ranging from 11 to 25 have been reported.<sup>1,2,31</sup>

The static dielectric tensor can be decomposed in the contributions of different modes as follows (see Ref. 32; we follow the notations of Ref. 23):

TABLE V. Components of mode-effective charge vectors  $Z_m^*$  and oscillator strength tensor  $S_m$  for each of the IR-active modes of HfSiO<sub>4</sub> and ZrSiO<sub>4</sub>. The description of the reported vector and tensor components corresponding to the two types of modes is given in the text. The components of the mode-effective charge vectors are given in units of  $|e|$ , where  $e$  is the electronic charge. The oscillator strengths are given in  $10^{-4}$  a.u. ( $1 \text{ a.u.} = 0.342036 \text{ m}^3/\text{s}^2$ ).

	HfSiO <sub>4</sub>		ZrSiO <sub>4</sub> <sup>a</sup>	
	$Z_m^*$	$S_m$	$Z_m^*$	$S_m$
$A_{2u}(1)$	6.85	7.39	7.68	10.06
$A_{2u}(2)$	3.78	4.24	2.76	2.64
$A_{2u}(3)$	6.60	11.22	6.71	11.50
$E_u(1)$	5.93	4.05	6.79	5.91
$E_u(2)$	2.94	1.70	3.51	2.71
$E_u(3)$	1.69	0.91	0.28	0.12
$E_u(4)$	7.21	14.02	7.37	14.69

<sup>a</sup>From Ref. 3.

$$\epsilon_{\alpha\beta}^0(\omega) = \epsilon_{\alpha\beta}^\infty + \sum_m \Delta\epsilon_{m,\alpha\beta} = \epsilon_{\alpha\beta}^\infty + \frac{4\pi}{\Omega_0} \sum_m \frac{S_{m,\alpha\beta}}{\omega_m^2}, \quad (1)$$

where  $\Omega_0$  is the volume of the primitive unit cell and  $S_{m,\alpha\beta}$  the mode-oscillator strength, which can be expressed in terms of the eigendisplacements and the Born effective charge tensors. We refer to Refs. 3 and 4 for explicit expressions. The contribution of the individual modes  $\Delta\epsilon_m$  to the static dielectric constant are indicated in Table IV. The largest contribution comes from the lowest-frequency mode.

We further analyze the decomposition of the static dielectric tensor using the mode-effective charge vectors, defined explicitly in Refs. 3 and 4. Each of these vectors is related to the global polarization resulting from the atomic displacements of a given phonon mode  $m$ . The nonzero components indicate the directions in which the mode is infrared active. In Table V, we present for each IR-active mode, the magnitude of the corresponding mode-effective charge vector (this vector is parallel and perpendicular to the tetragonal axis for  $A_{2u}$  and  $E_u$  modes, respectively), as well as the relevant component of the oscillator strength tensor (the parallel-parallel component for  $A_{2u}$  modes, and the perpendicular-perpendicular component for  $E_u$  modes).

The oscillator strengths and the mode-effective charges of HfSiO<sub>4</sub> are smaller than those of ZrSiO<sub>4</sub> [except for the  $A_{2u}(2)$  and  $E_u(3)$  modes]. The origin of this difference can be traced back to the Born effective charges and the eigendisplacements. Indeed, as discussed in Sec. III C, the Born effective charges of  $M=(\text{Hf}, \text{Zr})$  and Si atoms are smaller in HfSiO<sub>4</sub> than in ZrSiO<sub>4</sub>. Moreover, due to their heavier weight, the Hf atoms show smaller displacements than the Zr atoms.

Returning to the contributions to the static dielectric constant reported in Table IV, we observe that most of the contributions for HfSiO<sub>4</sub> are smaller than those for ZrSiO<sub>4</sub> [except those of the  $A_{2u}(2)$  and  $E_u(3)$  modes]. The contributions to  $\epsilon_0$  are affected by both the phonon frequencies and the

oscillator strengths. For instance, for the  $E_u(2)$  modes, not only the oscillator strengths of zircon are larger than those of hafnon, but also the relevant frequencies are lower in zircon than in hafnon, both trends contributing to increasing the dielectric constant. In other cases, when the frequencies show an opposite trend, the two effects compensate in part. For instance, for the  $A_{2u}(1)$  mode, the oscillator strength  $S_m$  in hafnon is 30% smaller than in zircon, but the corresponding contribution to  $\epsilon_0$  is only 20% smaller, since the associated frequency is about 10% larger. Finally, for the  $A_{2u}(2)$  and  $E_u(3)$  modes, the frequencies are very similar (these modes essentially involve displacements of the Si atoms and some of the O atoms) and therefore the oscillator strength governs the trend of the contributions to the static dielectric constant (larger in hafnon than in zircon).

Note that if the two materials had the same Born effective charge tensors and interatomic force constants, the sum of the various contributions to  $\epsilon_0$  should be identical.<sup>33</sup> In particular, the differences of the masses (which in turn influence the frequencies as discussed in Sec. III D) do not affect the overall static dielectric constant. Hence, the slightly higher static dielectric constant for zircon can be attributed to the slightly higher Born effective charges and lower interatomic force constants.

#### IV. CRYSTALLINE OXIDES

##### A. Structural properties

In the cubic phase,  $\text{HfO}_2$  and  $\text{ZrO}_2$  take the fluorite structure (space group  $Fm\bar{3}m$ ), which is fully characterized by a single lattice constant  $a$ . The  $M=(\text{Hf}, \text{Zr})$  atoms are in a face-centered-cubic structure and the O atoms occupy the tetrahedral interstitial sites associated with this fcc lattice. The unit cell contains one formula unit of  $MO_2$  with  $M=(\text{Hf}, \text{Zr})$ . The tetragonal phase (space group  $P4_2/nmc$ ) can be viewed as a distortion of the cubic structure obtained by displacing alternating pairs of O atoms up and down by an amount  $\Delta z$  along the  $z$  direction, and by applying a tetragonal strain. The resulting primitive cell is doubled compared to the cubic phase, including two formula units of  $MO_2$ . The tetragonal structure is completely specified by two lattice constants ( $a$  and  $c$ ) and the dimensionless ratio  $d_z = \Delta z/c$  describing the displacement of the O atoms. The cubic phase can be considered as a special case of the tetragonal structure with  $d_z=0$  and  $c/a=1$  (if the primitive cell is used for the tetragonal phase,  $c/a=\sqrt{2}$ ).

In Table VI, our calculated structural parameters for the cubic and tetragonal phases of  $\text{HfO}_2$  and  $\text{ZrO}_2$  are compared with the experimental values.<sup>34,35</sup> The agreement is very good: the errors on the lattice constants and the volumes are smaller than 2%, as is typical for LDA calculations. Our structural parameters also agree very well with the theoretical values found in Refs. 5 and 6.

##### B. Born effective charge tensors

In Table VII, we report the nonvanishing components of the calculated Born effective charge tensors of  $M=(\text{Hf}, \text{Zr})$  and O atoms in the cubic and tetragonal phases of hafnia and

TABLE VI. Structural parameters for the cubic (C) and tetragonal (T) phases of  $\text{HfO}_2$  and  $\text{ZrO}_2$ . The length unit is the Angstrom. The theoretical results for  $\text{ZrO}_2$  are those of Ref. 4. The experimental results for  $\text{HfO}_2$  are taken from Ref. 35, while those for  $\text{ZrO}_2$  are obtained by extrapolation to zero temperature using the thermal expansion data of Ref. 34.

	$\text{HfO}_2$		$\text{ZrO}_2^a$		
	Theor.	Expt.	Theor.	Expt.	
C					
	$a$	5.11	5.08	5.01	5.09
	Volume	33.36	32.77	31.44	32.97
	$d(M\text{-O})$	2.21	2.20	2.17	2.20
T					
	$a$	5.11	5.15	5.02	5.05
	$c$	5.17	5.29	5.09	5.18
	$d_z$	0.0310		0.0400	0.0574
	Volume	33.75	35.08	32.07	33.04
	$d(M\text{-O})$	2.13		2.07	2.05
		2.32		2.31	2.39

zirconia. Due to the symmetry of the cubic phase, the Born effective charge tensors of  $M=(\text{Hf}, \text{Zr})$  and O atoms are diagonal and isotropic. The value of  $Z^*$  is anomalously large for  $M=(\text{Hf}, \text{Zr})$  atoms compared to the nominal ionic charge  $Z=+4$ , indicating a mixed covalent-ionic bonding. In the tetragonal structure, the symmetry imposes that the Born effective charge tensor of  $M=(\text{Hf}, \text{Zr})$  atoms is diagonal and has only two independent components: parallel ( $Z_{\parallel}^*$ ) and perpendicular ( $Z_{\perp}^*$ ) to the  $c$  axis. The value of  $Z_{\perp}^*$  is identical to the one calculated for the cubic phase, while  $Z_{\parallel}^*$  is 6% and 10% smaller for  $\text{HfO}_2$  and  $\text{ZrO}_2$ , respectively. The Born effective charge tensor of the O atoms is also diagonal, but with three independent components. It is quite anisotropic compared to the cubic phase.

It is interesting to note that the Born effective charges of  $c\text{-HfO}_2$  are about 3% smaller (in absolute value) than those of  $c\text{-ZrO}_2$ . The comparison between the  $Z^*$  values of  $t\text{-HfO}_2$  and  $t\text{-ZrO}_2$  also deserves attention. In directions perpendicular to the  $c$  axis, the Born effective charges of the  $M=(\text{Hf}, \text{Zr})$  atoms compare in the same way as for the cubic phase, while the comparison for the Born effective charges of O

TABLE VII. Nonvanishing components of the calculated Born effective charge tensors of  $M=(\text{Hf}, \text{Zr})$  and O atoms in the cubic (C) and tetragonal (T) phases of  $\text{HfO}_2$  and  $\text{ZrO}_2$ . Only the diagonal elements are given, since the off-diagonal ones vanish by symmetry.

	Atom	$\text{HfO}_2$	$\text{ZrO}_2$
C			
	$M$	(+ 5.58+ 5.58+ 5.58)	(+ 5.74+ 5.74+ 5.74)
	O	(- 2.79- 2.79- 2.79)	(- 2.87- 2.87- 2.87)
T			
	$M$	(+ 5.57+ 5.57+ 5.24)	(+ 5.74+ 5.74+ 5.15)
	O	(- 3.22- 2.35- 2.62)	(- 3.51- 2.24- 2.57)

<sup>a</sup>From Ref. 4.

atoms shows an anisotropy in  $t$ -ZrO<sub>2</sub> stronger than that in  $t$ -HfO<sub>2</sub> by about 30% (the values of  $Z_{\perp}^*$  for  $t$ -HfO<sub>2</sub> are comprised between those of  $t$ -ZrO<sub>2</sub>). In the direction parallel to the  $c$  axis, the Born effective charges in  $t$ -HfO<sub>2</sub> are larger than in  $t$ -ZrO<sub>2</sub> by about 2%, showing an opposite trend with respect to the comparison for the cubic phase. The slightly different behavior between hafnia and zirconia can be related to the differences between the inner electronic shells of Hf and Zr, which lead to different polarizabilities.

Our calculated values for the various components of the Born effective charge tensors of ZrO<sub>2</sub> are essentially the same as those of Ref. 5. On the contrary, our results for HfO<sub>2</sub> may differ by as much as 5% from those of Ref. 6, which starts being significant and will affect the static dielectric constants (cf. Sec. IV D).

### C. Phonon frequencies at the $\Gamma$ point

The theoretical group analysis predicts the following irreducible representations of optical and acoustical zone-center modes for the cubic phase:

$$\Gamma = \underbrace{F_{2g}}_{\text{Raman}} \oplus \underbrace{F_{1u}}_{\text{IR}} \oplus \underbrace{F_{1u}}_{\text{Acoustic}}$$

and for the tetragonal phase:

$$\Gamma = \underbrace{A_{1g} \oplus 2B_{1g} \oplus 3E_g}_{\text{Raman}} \oplus \underbrace{A_{2u} \oplus 2E_u}_{\text{IR}} \oplus \underbrace{A_{2u} \oplus E_u}_{\text{Acoustic}} \oplus \underbrace{B_{2u}}_{\text{Silent}}.$$

Due to the nonvanishing components of the Born effective charge tensors, the dipole-dipole interaction leads to the splitting at the  $\Gamma$  point between the longitudinal and transverse optic (LO and TO, respectively) modes  $F_{1u}$  in the cubic phase, and  $E_u$  (perpendicular to the  $c$  axis) and  $A_{2u}$  (parallel to  $c$  axis) in the tetragonal phase.

Our calculated phonon frequencies and symmetry assignments (see the discussion in Ref. 4) are presented in Table VIII, where they are compared with those presented in Refs. 5 and 6.

It is very interesting to compare the phonon frequencies calculated for HfO<sub>2</sub> and ZrO<sub>2</sub> (see Table VIII). In Sec. III D, we have pointed out three possible origins for the variations of the frequencies in Hf and Zr based oxides: the structural changes, the Hf/Zr mass ratio (equal to 1.96), and the differences in interatomic force constants. By performing a similar analysis as for HfSiO<sub>4</sub> versus ZrSiO<sub>4</sub>, we find that the structural changes play a very minor role, in agreement with the intuition resulting from the very small variations observed in their structural parameters. As for the role of the mass ratio, it can clearly be evidenced in the modes in which the  $M=(\text{Hf}, \text{Zr})$  atoms move significantly more than O atoms: the  $B_{1g}(1)$  and  $E_g(1)$  modes of the tetragonal phase for which the frequencies vary by about 35%. On the contrary, the modes in which the  $M=(\text{Hf}, \text{Zr})$  atoms are not involved (i.e.,  $F_{2g}$  in the cubic phase, and  $A_{1g}$  and  $B_{2u}$  in the tetragonal phase), as well as those in which the O atoms move significantly more than the  $M=(\text{Hf}, \text{Zr})$  atoms [i.e.,  $F_{1u}$  in the cubic phase, and  $B_{1g}(2)$ ,  $E_g(2)$  and (3),  $A_{2u}$ , and  $E_u(1)$  and (2) in the tetragonal phase], should have frequencies

TABLE VIII. Fundamental frequencies of the cubic (C) and tetragonal (T) phases of HfO<sub>2</sub> and ZrO<sub>2</sub> (in cm<sup>-1</sup>) with their symmetry assignments. For hafnia, our results for the TO infrared modes are compared with those of Ref. 6; for zirconia, the comparison is between the results of Refs. 4 and 5.

Mode	HfO <sub>2</sub>		ZrO <sub>2</sub>	
	This work	Ref. 6	Ref. 4	Ref. 5
<b>C</b>				
Raman				
$F_{2g}$	579		596	
Infrared				
$F_{1u}$ (TO)	285	286	280	258
$F_{1u}$ (LO)	630		677	
<b>T</b>				
Raman				
$A_{1g}$	218		259	
$B_{1g}(1)$	244		331	
$B_{1g}(2)$	582		607	
$E_g(1)$	110		147	
$E_g(2)$	479		474	
$E_g(3)$	640		659	
Infrared				
$A_{2u}$ (TO)	315	384	339	334
$A_{2u}$ (LO)	621		664	
$E_u$ (TO1)	185	117	153	154
$E_u$ (LO1)	292		271	
$E_u$ (TO2)	428	536	449	437
$E_u$ (LO2)	669		734	
Silent				
$B_{2u}$	665		673	

very similar for HfO<sub>2</sub> and ZrO<sub>2</sub>. This is indeed what is observed in most of the cases. However, in a few cases, the differences in the interatomic force constants dominate, leading to noticeable changes in the frequencies. For instance, for the  $A_{1g}$  and  $E_u(1)$  modes in the tetragonal phase, variations of 19% and 17% are obtained, respectively.

Our calculated frequencies for zirconia are in good agreement with those of Ref. 5. The agreement is excellent for the tetragonal phase (less than 3% difference) and quite reasonable in the cubic phase (about 10% discrepancy for the  $F_{1u}$ ). On the contrary, for hafnia, the matching with Ref. 6 is almost perfect for the cubic phase (less than 1% difference), while, for the tetragonal phase, very important differences occur in some cases. In particular, for the  $E_u(1)$  mode, we find a value 37% larger than in Ref. 6. These differences will lead to important discrepancies in the static dielectric constant because the frequency appears as a square factor in Eq. (1) (cf. Sec. IV D).

### D. Dielectric permittivity tensors

In the cubic phase, the electronic ( $\epsilon_{\infty}$ ) and static ( $\epsilon_0$ ) permittivity tensors are diagonal and isotropic. In the tetragonal crystal, these tensors are still diagonal by symmetry, but have two independent components  $\epsilon_{\parallel}$  and  $\epsilon_{\perp}$ , parallel and

TABLE IX. Electronic and static dielectric tensors for the cubic (C) and tetragonal (T) phases of HfO<sub>2</sub> and ZrO<sub>2</sub>. The contributions of the different phonon modes to the static dielectric tensor are also indicated, the corresponding results of Ref. 6 for hafnia and of Ref. 5 for zirconia are reported between parentheses. For the cubic phase, the tensors are diagonal and isotropic. The phonon mode contribution to  $\epsilon_0^{\parallel}$  comes from the IR-active  $F_{1u}$  mode. For the tetragonal phase, the tensors are also diagonal but they have different components parallel ( $\parallel$ ) and perpendicular ( $\perp$ ) to the  $c$  axis. The phonon mode contribution to  $\epsilon_0^{\parallel}$  comes from the IR-active  $A_{2u}$  mode, while the contributions to  $\epsilon_0^{\perp}$  come from the two IR-active  $E_u$  modes.

	HfO <sub>2</sub>		ZrO <sub>2</sub> <sup>a</sup>	
C				
$\epsilon_{\infty}$	5.37		5.74	
$\Delta\epsilon$	20.80	(23.9)	27.87	(31.8)
$\epsilon_0$	26.17		33.61	
T				
	$\parallel$	$\perp$	$\parallel$	$\perp$
$\epsilon_{\infty}$	5.13	5.39	5.28	5.74
$\Delta\epsilon_1$	14.87	(10.7)	22.34	(88.9)
$\Delta\epsilon_2$		5.08	(3.4)	6.91
$\epsilon_0$	20.00	32.81	20.31	48.13

<sup>a</sup>From Ref. 4.

perpendicular to the  $c$  axis, respectively. In Table IX, the calculated values of  $\epsilon_{\infty}$  and  $\epsilon_0$  are reported for the cubic and the tetragonal phases of hafnia and zirconia. In the tetragonal phase, the  $\epsilon_{\infty}$  tensor is only slightly anisotropic with about 5% and 10% difference between the parallel and perpendicular values for  $t$ -HfO<sub>2</sub> and  $t$ -ZrO<sub>2</sub>, respectively. On the contrary, the  $\epsilon_0$  tensor is highly anisotropic: the value of  $\epsilon_0$  in the direction parallel to the  $c$  axis is 1.6 and 2.4 times smaller than that in the perpendicular direction for  $t$ -HfO<sub>2</sub> and  $t$ -ZrO<sub>2</sub>, respectively. While the values of  $\epsilon_{\infty}$  for the cubic and tetragonal phases are very close, those of  $\epsilon_0$  differ significantly.

The contribution of the individual modes  $\Delta\epsilon_m$  to the static dielectric constants, as defined in Eq. (1), are presented in Table IX, where the cases of hafnia and zirconia can be compared. The comparison is extended in Table X, where we reported, for each IR-active mode, the relevant component of the oscillator strength tensor. This tensor is isotropic for the  $F_{1u}$  mode in the cubic phase, while, for the tetragonal phase, we indicate the parallel-parallel component for the  $A_{2u}$  mode, and the perpendicular-perpendicular component for the  $E_u$  modes. We also give the magnitude of the mode-effective charge vector, which is parallel and perpendicular to the tetragonal axis for  $A_{2u}$  and  $E_u$  modes, respectively, while it has an arbitrary orientation for the  $F_{1u}$  mode. The atomic motions associated to these vibrational modes have been described in detail in the literature.<sup>36–38</sup>

In Table X, it can be observed that the oscillator strengths and the mode-effective charges of HfO<sub>2</sub> are smaller than those of ZrO<sub>2</sub>. This can be related to the behavior of the Born effective charges and the eigendisplacements, the two quantities determining the oscillator strengths  $S_{m,\alpha\beta}$ .<sup>3,4</sup> On the one hand, as discussed in Sec. IV B, the Born effective

TABLE X. Components of mode-effective charge vectors  $Z_m^*$  and oscillator strength tensor  $S_m$  for each of the IR-active modes of the cubic (C) and tetragonal (T) phases of HfO<sub>2</sub> and ZrO<sub>2</sub>. The description of the reported vector and tensor components corresponding to the different modes is given in the text. For the oscillator strengths, the results of Ref. 6 for hafnia and of Ref. 5 for zirconia are also indicated between parentheses (Ref. 39). Same units as in Table V.

		HfO <sub>2</sub>		ZrO <sub>2</sub> <sup>a</sup>	
	$Z_m^*$	$S_m$	$Z_m^*$	$S_m$	
C					
	$F_{1u}$	5.82	6.31	(6.88)	6.42
T					
	$A_{2u}$	7.71	11.10	(11.53)	8.14
	$E_u(1)$	5.75	5.76	(8.71)	5.95
	$E_u(2)$	5.91	7.03	(7.00)	6.99

<sup>a</sup>From Ref. 4.

charges are globally smaller in HfO<sub>2</sub> than in ZrO<sub>2</sub>. On the other hand, the Hf atoms show smaller displacements than the Zr atoms due to their heavier mass (see Sec. IV C).

If one now considers the contributions to the static dielectric constant reported in Table IX, it clearly appears that the contributions for HfO<sub>2</sub> are smaller than those for ZrO<sub>2</sub>. However, despite the fact that in all cases the oscillator strengths are smaller for hafnia than for zirconia, two different situations can be distinguished depending on the behavior of the phonon frequencies. On one hand, for the  $E_u(1)$  mode, the frequency for HfO<sub>2</sub> is larger than for ZrO<sub>2</sub>. In this case, the contribution for ZrO<sub>2</sub> is noticeably larger (about 60%) than for HfO<sub>2</sub>. For the  $F_{1u}$  mode in the cubic phase, the situation is very similar though the frequency does not change very much. On the other hand, for the  $A_{2u}$  mode, the frequency changes in the opposite way. As a result, the increase by 6% of the oscillator strengths is almost completely compensated by the raise of 7% in the frequency: in the end, there only remains a 1% difference between the contributions for HfO<sub>2</sub> and ZrO<sub>2</sub>. For the  $E_u(2)$  mode, the raise of 5% in the frequency only slightly attenuates the 15% increase of the oscillator strengths.

Globally, the differences in the static dielectric constants for zirconia and hafnia can be related to the Born effective charge tensors and the interatomic force constants, as discussed at the end of Sec. III E. On the one hand, for the cubic phase and for the perpendicular component in the tetragonal phase, the two effects combine and lead to a large increase of the static dielectric constants in ZrO<sub>2</sub>. The latter is essentially due to lower interatomic force constants, since the effective charges are higher by only 3%. On the other hand, for the parallel component of the tetragonal phase, the lowering of the interatomic force constants in zirconia is compensated by a reduction by 2% of the effective charges.

For comparison, we also reported in Tables IX and X corresponding results obtained in Refs. 5 and 6. While our results for ZrO<sub>2</sub> are in reasonable agreement with the results of Ref. 5, we find noticeable differences with respect to Ref. 6 for the contributions to the static dielectric constants of

HfO<sub>2</sub>. The most impressive variation is observed for the  $E_u(1)$  mode in the tetragonal phase which gives the first contribution to  $\epsilon_0^\perp$ . We find a value about four times smaller than in Ref. 6. This discrepancy can be traced back to the relevant vibrational frequency which is 37% higher in our work (see Sec. IV C) and, to a lesser extent, to the difference in the corresponding component of the Born effective charge tensor which we find to be 5% smaller (see Sec. IV B). In terms of the oscillator strength tensors (Table X), the comparison is very similar. The agreement with Ref. 5 is very good for zirconia while there are significant divergences with Ref. 6 for hafnia. Again, the largest difference (33%) is found for the  $E_u(1)$  mode of the tetragonal phase. It is difficult to identify the origin for the differences between our results and those in Refs. 5 and 6, since very distinct technical ingredients have been used in the two calculations. For instance, our approach is based on a perturbational framework involving norm-conserving pseudopotentials. At variance, the results in Refs. 5 and 6 were obtained with a Berry phase formulation for the polarization, applied to an ultrasoft pseudopotential scheme.

## V. CONCLUSION

Using density-functional theory, we have investigated the structural, electronic, dynamical, and dielectric properties of Hf and Zr silicates and oxides, which are the most promising high- $\kappa$  alternatives to the conventional SiO<sub>2</sub> gate dielectric. We have considered the two crystalline silicates (hafnon and zircon), and the cubic and tetragonal phases of the Hf and Zr oxides.

In all the investigated systems, the parameters of the relaxed atomic structures are found to be in very good agreement with experimental ones (when available). An important anisotropy has been evidenced in the Born effective charge tensors. For some directions, these effective charges are found to be larger than the nominal ionic charge, indicating a mixed covalent-ionic bonding between  $M=(\text{Hf}, \text{Zr})$  and O

atoms, and between Si and O atoms. We have discussed the effective charges focusing on the changes between the systems containing hafnium and those containing zirconium. For the silicates, we have also analyzed the electronic properties; in particular, the electronic density of states has been presented. The states at the top of the valence band have been found to be mainly of O  $2p$  character with some mixing of Si and  $M=(\text{Hf}, \text{Zr})$  orbitals. This confirms that the bonding in these compounds is of mixed covalent-ionic character.

For both of the silicates and of the oxides, the phonon frequencies at the center of the Brillouin zone have been computed and found to be in very good agreement with available experimental data. Differences between the vibrational frequencies of Hf and Zr compounds have been rationalized in terms of changes in the structural parameters, difference in mass between Hf and Zr, and variations in the interatomic force constants.

The electronic and static dielectric permittivity constants have been computed, and a detailed analysis of the contributions of individual vibrational modes has been performed, including the computation of mode-effective charges and oscillator strengths. Our results do not confirm the unusually high value for the static dielectric constant in directions perpendicular to the tetragonal axis for tetragonal HfO<sub>2</sub>, as found in a recent calculation.<sup>6</sup> The static dielectric constants calculated in this work indicate an overall similarity between Hf and Zr compounds as far as the trends are concerned, which is essentially due to the chemical homology of hafnium and zirconium. The Zr compounds generally show higher static dielectric constants, due to higher Born effective charges and lower interatomic force constants.

Using the microscopic scheme which relates the dielectric constants to the underlying microstructure,<sup>8</sup> we can extrapolate from our results that the same conclusions hold for amorphous Hf and Zr oxides and silicates. In summary, there does not seem to be a specific geometry (e.g., the tetragonal phase) that would contribute to increasing the dielectric constant.

<sup>1</sup>G.D. Wilk, R.M. Wallace, and J.M. Anthony, *J. Appl. Phys.* **89**, 5243 (2001).

<sup>2</sup>G.D. Wilk and R.M. Wallace, *Appl. Phys. Lett.* **74**, 2854 (1999); G.D. Wilk and R.M. Wallace, *ibid.* **76**, 112 (2000); G.D. Wilk, R.M. Wallace, and J.M. Anthony, *J. Appl. Phys.* **87**, 484 (2000).

<sup>3</sup>G.-M. Rignanese, X. Gonze, and A. Pasquarello, *Phys. Rev. B* **63**, 104305 (2001).

<sup>4</sup>G.-M. Rignanese, F. Detraux, X. Gonze, and A. Pasquarello, *Phys. Rev. B* **64**, 134301 (2001).

<sup>5</sup>X. Zhao and D. Vanderbilt, *Phys. Rev. B* **65**, 075105 (2002).

<sup>6</sup>X. Zhao and D. Vanderbilt, *Phys. Rev. B* **65**, 233106 (2002).

<sup>7</sup>V. Fiorentini and G. Gulleri, *Phys. Rev. Lett.* **89**, 266101 (2002).

<sup>8</sup>G.-M. Rignanese, F. Detraux, X. Gonze, A. Bongiorno, and A. Pasquarello, *Phys. Rev. Lett.* **89**, 117601 (2002).

<sup>9</sup>K. Parlinski, Z.-Q. Li, and Y. Kawazoe, *Phys. Rev. Lett.* **78**, 4063 (1997).

<sup>10</sup>F. Detraux, Ph. Ghosez, and X. Gonze, *Phys. Rev. Lett.* **81**,

3297 (1998).

<sup>11</sup>The electron configuration of hafnium is  $4f^{14}5d^26s^2$  while it is  $4d^25s^2$  for zirconium. In the Periodic Table, the inner transition (rare-earth) elements immediately preceding Hf add electrons to the inner  $4f$  shell from element No. 58, cerium, to No. 71, lutetium. Because the nuclear charge increases while no additional outer shells are filled, there is a contraction in the atomic size. Consequently, the element No. 72, hafnium, has a slightly smaller atomic size than element No. 40, zirconium, the group IVB element in the preceding row. This results in the so-called lanthanide contraction. The atomic radii of Hf and Zr are close to each other: 1.44 and 1.45 Å, respectively (Ref. 40). They also have quasi-identical ionic radii ( $M^{4+}$ ) 0.78 for Hf and 0.79 Å for Zr, respectively (Ref. 41). Their electronegativity values are almost equal 1.23 for hafnium and 1.22 for zirconium (Ref. 42).

<sup>12</sup>J.A. Speer and B.J. Cooper, *Am. Mineral.* **67**, 804 (1982).

<sup>13</sup>X. Gonze, J.-M. Beuken, R. Caracas, F. Detraux, M. Fuchs, G.-M.

- Rignanese, L. Sindic, M. Verstraete, G. Zerah, F. Jollet, M. Torrent, A. Roy, M. Mikami, Ph. Ghosez, J.-Y. Raty, and D.C. Allan, *Comput. Mater. Sci.* **25**, 478 (2002). <http://www.abinit.org>
- <sup>14</sup>J.P. Perdew and Y. Wang, *Phys. Rev. B* **45**, 13 244 (1992).
- <sup>15</sup>D.M. Ceperley and B.J. Alder, *Phys. Rev. Lett.* **45**, 566 (1980).
- <sup>16</sup>N. Troullier and J.L. Martins, *Phys. Rev. B* **43**, 1993 (1991).
- <sup>17</sup>M. Teter, *Phys. Rev. B* **48**, 5031 (1993).
- <sup>18</sup>L. Kleinman and D.M. Bylander, *Phys. Rev. Lett.* **48**, 1425 (1982).
- <sup>19</sup>Z. Mursic, T. Vogt, H. Boysen, and F. Frey, *J. Appl. Crystallogr.* **25**, 519 (1992).
- <sup>20</sup>Ph. Ghosez, J.-P. Michenaud, and X. Gonze, *Phys. Rev. B* **58**, 6224 (1998).
- <sup>21</sup>C. Lee and X. Gonze, *Phys. Rev. Lett.* **72**, 1686 (1994).
- <sup>22</sup>C. Lee, Ph. Ghosez, and X. Gonze, *Phys. Rev. B* **50**, 13 379 (1994).
- <sup>23</sup>X. Gonze and C. Lee, *Phys. Rev. B* **55**, 10 355 (1997).
- <sup>24</sup>X. Gonze, J.-C. Charlier, D.C. Allan, and M.P. Teter, *Phys. Rev. B* **50**, 13 035 (1994).
- <sup>25</sup>P. Giannozzi, S. de Gironcoli, P. Pavone, and S. Baroni, *Phys. Rev. B* **43**, 7231 (1991).
- <sup>26</sup>J.H. Nicola and H.N. Rutt, *J. Phys. C* **7**, 1381 (1974).
- <sup>27</sup>P.W.O. Hoskin and K.A. Rodgers, *Eur. J. Solid State Inorg. Chem.* **23**, 1111 (1996).
- <sup>28</sup>P. Dawson, M.M. Hargreave, and G.R. Wilkinson, *J. Phys. C* **4**, 240 (1971).
- <sup>29</sup>F. Gervais, B. Piriou, and F. Cabannes, *J. Phys. Chem. Solids* **34**, 1785 (1973).
- <sup>30</sup>C. Pecharrómán, M. Ocaña, P. Tartaj, and C.J. Serna, *Mater. Res. Bull.* **29**, 417 (1994).
- <sup>31</sup>A. Callegari, E. Cartier, M. Gribelyuk, H.F. Okorn-Schmidt, and T. Zabel, *J. Appl. Phys.* **90**, 6466 (2001).
- <sup>32</sup>A.A. Maradudin, E.W. Montroll, G.H. Weiss, and I.P. Ipatova, in *Solid State Physics: Advances in Research and Applications*, edited by H. E. Ehrenreich, F. Seitz, and D. Turnbull (Academic, New York, 1971), Suppl. 3, Chap. 4.
- <sup>33</sup>See for instance Eq. (50) of Ref. 23. Note however that each of the mode contributions can differ individually. It is only their sum that is identical.
- <sup>34</sup>P. Aldebert and J.P. Traverse, *J. Am. Ceram. Soc.* **68**, 34 (1985).
- <sup>35</sup>J. Wang, H.P. Li, and R. Stivens, *J. Mater. Sci.* **27**, 5397 (1992).
- <sup>36</sup>C. Pecharrómán, M. Ocaña, and C.J. Serna, *J. Appl. Phys.* **80**, 3479 (1996).
- <sup>37</sup>K. Negita, *Acta Metall.* **37**, 313 (1989).
- <sup>38</sup>K. Negita and H. Takao, *J. Phys. Chem. Solids* **50**, 325 (1989).
- <sup>39</sup>It can easily be demonstrated that the oscillator strength components  $S_{m,\alpha\beta}$  used in the present work are related to the mode-effective charges  $\tilde{Z}_{m,\alpha}^*$  used in Refs. 5 and 6 by:  $S_{m,\alpha\beta} = \tilde{Z}_{m,\alpha}^* \tilde{Z}_{m,\beta}^* / M_0$ , where  $M_0 = 1$  amu. Note also that the mode-effective charges  $Z_{m,\alpha}^*$  used in this study and which are defined in Refs. 3 and 4 differ from the  $\tilde{Z}_{m,\alpha}^*$  of Refs. 5 and 6.
- <sup>40</sup>R.C. Weast, *CRC Handbook for Chemistry and Physics*, 65th ed. (CRC Press, Boca Raton, FL, 1985), p. 165.
- <sup>41</sup>R. Ruh and P.W.R. Corfield *J. Am. Ceram. Soc.* **53**, 126 (1970).
- <sup>42</sup>E.J. Little and M.M. Jones, *J. Chem. Educ.* **37**, 231 (1960).